JOURNAL OF GEOPHYSICAL RESEARCH, VOL. 112, D23101, doi:10.1029/2007JD008613, 2007

Heat budget of the East Antarctic lower atmosphere derived from a regional atmospheric climate model

W. J. van de Berg,[1] M. R. van den Broeke,[1] and E. van Meijgaard[2]

Received 5 March 2007; revised 18 July 2007; accepted 9 August 2007; published 4 December 2007.

[1] The heat budget of the lower East Antarctic atmosphere is calculated using output from a regional atmospheric climate model. The climatology of this model compares well with observations, although the surface energy budget shows an underestimation of the downwelling longwave radiation and an overestimation of the sensible heat flux. The winter atmospheric boundary layer over Antarctica is characterized by a strong surface inversion, due to longwave cooling of the surface. The longwave radiation loss is balanced by heat extracted from the atmosphere by turbulent mixing, which in turn is compensated by large-scale horizontal and vertical heat advection. Above the boundary layer, net longwave cooling is balanced by subsidence. In the coastal margin, latent heat release from condensation is a significant heat budget component. In summer, the surface is near radiative balance, resulting in a weak surface inversion. As a result, cooling by turbulent mixing and heating by advection in the atmospheric boundary layer are largely reduced. Absorption of shortwave radiation is a small heating source throughout the atmosphere, reducing the importance of advection above the boundary layer. Net longwave cooling and heating by condensation remain unchanged compared to winter.

Citation: van de Berg, W. J., M. R. van den Broeke, and E. van Meijgaard (2007), Heat budget of the East Antarctic lower atmosphere derived from a regional atmospheric climate model, *J. Geophys. Res.*, *112*, D23101, doi:10.1029/2007JD008613.

1. Introduction

[2] Antarctica is covered by the largest ice sheet on Earth, and its sheer size permits it to create its own climate. The most prominent elements of the climate of East Antarctica are the near-surface temperature inversion of up to 30 K [*Connolley*, 1996], and the katabatic wind in the boundary layer [*Parish and Bromwich*, 1987]. During winter, in the absence of solar radiation, both phenomena are most prominent and persistent.

[3] The climate of the atmospheric boundary layer (ABL) of East Antarctica is mainly forced by the negative surface radiation budget, which cools the surface of the Antarctic ice sheet. This imbalance is largest during the polar winter night; the surface radiation budget becomes slightly positive during the short summer [*van den Broeke et al.*, 2004]. *Cerni and Parish* [1984] explained the strength and depth of the inversion as a balance between net longwave emission and sensible heat transport. Over sloping surfaces, the cold near-surface air introduces a horizontal pressure gradient force, which drives the katabatic winds. Even over the gentle slopes of the East Antarctic plateau, the katabatic forcing is significant [*Brost and Wyngaard*, 1978]. The near-surface winds are enhanced by the large-scale forcing, which is directed parallel to the katabatic forcing for most of East Antarctica [*van den Broeke et al.*, 2002; *Parish and Cassano*, 2003].

[4] The heat budget governs the atmospheric temperature evolution. Several studies have addressed the momentum budget of the East Antarctic lower atmosphere [*van den Broeke et al.*, 2002; *van den Broeke and van Lipzig*, 2003], or specific aspects such as a pure katabatic flow [*Renfrew*, 2004]. However, only few quantitative analyses of the heat budget have yet been provided. *King et al.* [2001] analyzed the components of the ABL heat budget in order to assess mixing parameterizations. Furthermore, *van As and van den Broeke* [2006] deal with the heat budget of the summertime ABL over the Antarctic interior.

[5] Analysis of the heat budget does not directly provide insight in the dependency of temperature on measurable quantities such as katabatic or large-scale wind speed, cloud cover and optical thickness. Rather, it provides the physical connection between these quantities and atmospheric temperature. For example, a change in cloud thickness would alter the net longwave cooling at that level, but also affects the surface radiative balance and thus reduces the cooling of the boundary layer by turbulent mixing.

[6] In the ABL, the heat budget directly interacts with the surface energy budget, but it is also influenced by large-scale dynamical processes. Above the ABL, heat advection is a major driving mechanism. Significant heat advection on climatological timescales requires persistent temperature gradients along the dominant wind direction, and these temperature gradients can only be maintained by other processes, such as longwave radiative cooling.

[1] Institute for Marine and Atmospheric Research Utrecht, University of Utrecht, Utrecht, Netherlands.
[2] Royal Dutch Meteorological Institute, De Bilt, Netherlands.

0148-0227/07/2007JD008613$09.00

[7] In this paper, we present the climatological heat budget of the lower East Antarctic atmosphere as estimated from output of an atmospheric climate model. In the end, these results can help explain temperature change in the Antarctic, as reported by *van den Broeke and van Lipzig* [2004] and *Turner et al.* [2005]. However, the analysis of temporal changes in the heat budget is postponed to a forthcoming paper.

[8] Although atmospheric heat budget terms could be directly measured in theory, it is unfeasible in practice. We therefore use output from a regional climate model to quantify the heat budget of the Antarctic lower atmosphere. Atmospheric models solve the heat budget equation in order to calculate the temperature evolution in time.

[9] Here, we limit ourselves to mean winter and summer heat budgets over East Antarctica and the surrounding seas. In contrast to West Antarctica and the Antarctic Peninsula, East Antarctica has a rather uniform topography, allowing for a grouping of the heat budget terms in elevation bins over the ice sheet and distance bins over the coastal seas.

[10] In the next section, a brief description of the model is given. In section 3, the heat budget is derived and calculation methods are presented. In section 4, the model climatology is evaluated. Section 5 presents the heat budget results, starting with the climatology of East Antarctica, and after that the winter and summer heat budgets.

2. Model Description

[11] For this study, model output is used from the regional atmospheric climate model RACMO2/ANT This model is especially adapted for Antarctic conditions. It consists of the atmospheric dynamics of the High-Resolution Limited Area Model (HiRLAM), version 5.0.6. [*Undén et al.*, 2002] and the physical processes package from the European Centre for Medium-Range Weather Forecasts (ECMWF), cycle CY23R4 [*White*, 2001].

[12] Several physical parameterisations within RACMO2/ANT have been changed to better represent Antarctic conditions. The snow albedo parameterisation of *van den Hurk and Viterbo* [2003] was implemented. For freezing conditions, the albedo decay in this parameterization is diminished proportional with the fourth power of the temperature. As a result, the albedo of snow remains almost constant below $-10°C$. Furthermore, the surface roughness length for momentum was reduced [*Reijmer et al.*, 2004], and the expression presented by *Andreas* [1987] was applied to calculate the surface roughness lengths of heat and moisture over snow surfaces. A four layer snow model was added to improve subsurface heat fluxes into the snow pack. These adjustments and their positive effect on the boundary layer, together with the setup of RACMO2/ANT are described by *Reijmer et al.* [2005]. Since that publication, a correction has been made to include fractional sea ice cover. Horizontal diffusion of moisture has been decreased by a factor of ten in order to reduce artificial uphill moisture transport [*Lenderink et al.*, 2003]. Concentrations of CO_2 and other trace gasses have been varied following *Intergovernmental Panel on Climate Change* [2001]. Erratic rain generation for subzero temperatures has been corrected, taking in account the additional energy release [*van de Berg et al.*, 2006].

Table 1. List of Physical Parameters and Constants Used

Symbol	Name, Unit
T	temperature, K
θ	potential temperature, K
p	pressure, Pa
ρ	density, kg m^{-3}
$\vec{u}$	3-D velocity field, m s^{-1}
u, v, w	cross-slope, along-slope and vertical wind, m s^{-1}
c_p	heat capacity of air, J $K^{-1}kg^{-1}$
J	external heating term, J s^{-1} kg^{-1}

[13] The integration with RACMO2/ANT has been performed with a horizontal resolution of ~55 km and 40 levels in the vertical, of which the lowest is about 10 m above the surface. The model employs a hybrid vertical coordinate. ECMWF Reanalysis (ERA-40) fields forced the model at the lateral boundaries and provided sea surface temperature and sea ice fraction. Model results prior to 1980 have been excluded from the analysis because of the reduced quality of ERA-40 in high southern latitudes [*Bromwich and Fogt*, 2004; *Sterl*, 2004; *van de Berg et al.*, 2005]. The model integration has been extended until the end of 2004 with lateral forcings and sea surface boundary conditions taken from ECMWF operational analysis.

[14] We used a regional climate model for two reasons. Firstly, the model interior of RACMO2/ANT evolves freely without intermediate model reinitializations, thus the model heat budget components all link to physical processes in the interior model domain. In contrast, intermediate model reinitializations or assimilation methods, as used in ECMWF products, have a systematic temperature effect. Although the heat budget still closes, this represents an additional spurious heat budget term that has no physical meaning. Secondly, as discussed in the next section, flux profiles of numerous parameters are required for the analysis of the heat budget. The standard archived model output of global circulation models is insufficient in this respect for a heat budget analysis.

3. Heat Budget

3.1. Derivation of Temperature Tendency Equation

[15] Conservation of energy in the atmosphere can be formulated as [*Holton*, 1992]

$$c_p \frac{\mathrm{d}T}{\mathrm{d}t} - \frac{1}{\rho}\frac{\mathrm{d}p}{\mathrm{d}t} = J. \tag{1}$$

[16] Physical parameters and constants are listed in Table 1. The left hand side of equation (1) represents the adiabatic interaction between temperature and pressure, the right hand side represents diabatic processes. The local temperature tendency (*LTT*) and the resolved advection (*RAdv*) can be separated in the adiabatic interaction, since

$$\frac{\mathrm{d}T}{\mathrm{d}t} - \frac{1}{\rho c_p}\frac{\mathrm{d}p}{\mathrm{d}t} = \underbrace{\frac{\partial T}{\partial t} - \frac{1}{\rho c_p}\frac{\partial p}{\partial t}}_{LTT} + \underbrace{\vec{u}\cdot\left(\nabla T - \frac{1}{\rho c_p}\nabla p\right)}_{RAdv}. \tag{2}$$

[17] An atmospheric model captures only flow patterns coarser than the model resolution: the advection simulated

by a model thus only represents contributions from the large-scale flow. Within this resolved large-scale advection, "horizontal" (*AdvH*) and vertical (*AdvV*) advection have been separated. "Horizontal" advection is not calculated on levels of constant height, but along η-levels. The η-coordinate system was retained for this analysis, because of its favorable characteristic that low-level winds follow the surface, independent of the surface slope, while the free-atmosphere circulation, which tend to follow pressure levels, is mostly "horizontal" too.

[18] On the right hand side of equation (1), J represents external heating processes, numerical filtering (K) and small-scale heat advection. In the atmosphere, external heating processes are absorption of shortwave radiation (*SWD*), absorption and emission of longwave radiation (*LWD*), and heat exchange by various water phase changes (Q) like condensation and evaporation or melt of precipitation. The radiation fluxes of shortwave and longwave are abbreviated to *SW* and *LW*, respectively.

[19] Horizontal temperature variations with a length scale similar to the model resolution are numerically filtered, to prevent numerical instabilities. This diffusion K can be considered as implicit advection and consists of a ∇^4 filter; it is calculated in the model dynamics section.

[20] The exchange of heat by subgrid-scale vertical air motion is parameterized in the model physics package. The ECMWF physics package makes a distinction between vertical turbulent mixing and convection. Turbulent mixing represents the exchange of heat between vertical levels and with the surface through the sensible heat flux (*SHF*). Sensible heat divergence (*SHD*) represents the local heating or cooling due to convergence or divergence of *SHF*. Convection represents transport of energy by rising air parcels in a conditionally unstable atmosphere and has no direct interaction with the surface. Similar to turbulent mixing, local heating or cooling by convection (*CHD*) represents convergence or divergence of the convective heat flux (*CHF*).

[21] Summarizing, in our atmospherical model conservation of energy is expressed by the following heat budget equation

$$\frac{\partial T}{\partial t} - \frac{1}{\rho c_p}\frac{\partial p}{\partial t} = -\vec{u}\cdot\left(\nabla T - \frac{1}{\rho c_p}\nabla p\right) + K - \frac{1}{\rho c_p}\frac{\partial SW}{\partial z} - \frac{1}{\rho c_p}\frac{\partial LW}{\partial z} - \frac{1}{\rho c_p}\frac{\partial SHF}{\partial z} - \frac{1}{\rho c_p}\frac{\partial CHF}{\partial z} + Q, \quad (3)$$

which is abbreviated in this paper as

$$LTT = AdvV + AdvH + K + SWD + LWD + SHD + CHD + Q. \quad (4)$$

3.2. Calculation of Individual Terms

[22] The heat budget terms in equation (4) are calculated using monthly averaged diagnostic model profiles of *SW*, *LW*, *SHF*, *LHF* and 6-hourly model states of T, Q, p and cloud content. In order to validate the truncation to 6-hourly intervals for advection and monthly intervals for the external heating processes, the outcome is compared to a 1-year (a) control run in which all temperature tendency terms were explicitly stored. Using the tendencies of the temperature and pressure, the resolved advection could be exactly determined. The resolved advection that is computed using 6-hourly instantaneous wind, temperature and pressure fields, shows a good match with the control run. Consequently, large-scale energy transport owing to variability on timescales shorter than 6 h is found negligible.

[23] The vertical profiles of *SW*, *LW*, *SHF* and *CHF* are derived from monthly accumulated profiles. The temperature change by Q is calculated afterward using the vertical fluxes of solid and liquid precipitation and the temporal change and advection of cloud content. This estimate of Q is successfully validated with the control run, in which accumulated water phase change profiles have been stored. *SWD*, *LWD*, *SHD*, C and Q thus obtained, are found to agree with the temperature tendency for the control run, with two exceptions. Energy fluxes induced by turbulent mixing at the top and base of stratiform clouds, usually occurring over the Southern Ocean, have not been included in the diagnostic output, which locally leads to an imbalance in the heat budget, but one that is always less than 1 K per day. Furthermore, during situations with strong winds and a very large downward *SHF*, the diagnostic flux exceeds the model flux near the surface. A maximum underestimation of 2 K per day is found near the surface in the escarpment zone.

[24] Finally, diffusion (K) is determined as a residual. Analysis of the 1-year control run shows that on longer timescales, the contribution of K to the heat budget is only significant over steep terrain. Note that errors in the diagnostics of turbulent mixing, as described above, also leads to residuals in the heat budget, and thus contribute to the presented value of K. These occasions will be discussed.

4. Model Evaluation

[25] Heat budget terms do not represent directly observable quantities. Therefore the calculated heat budget can only be evaluated indirectly, using observable quantities such as temperature, wind and surface radiation fluxes. Most meteorological observation sites are located along the coast of East Antarctica and the Antarctic Peninsula. West Antarctica and the East Antarctic plateau are nearly devoid of stations, as is the Southern Ocean.

[26] A thorough evaluation of the model climatology is presented by *Reijmer et al.* [2005]. They compared RACMO2/ANT output with 10 m wind speed and 2 m temperatures measured at (automatic) weather stations, and radiosonde data of wind and temperature at Neumayer and South Pole stations. They concluded that near-surface winds and temperatures are well represented in RACMO2/ANT and that the model performs better than ERA-40 in this respect. The model also represents the radiosonde data well. They did not observe a seasonal variation of the model performance.

[27] The adjustments that have been added to the physics package of RACMO2/ANT since the study of *Reijmer et al.* [2005], namely the reduction of horizontal moisture diffusion, the time varying of trace gas concentrations, and the correction of subzero rain generation, have an insignificant impact on model climatology. However, the inclusion of fractional sea ice cover introduces a near surface tempera-

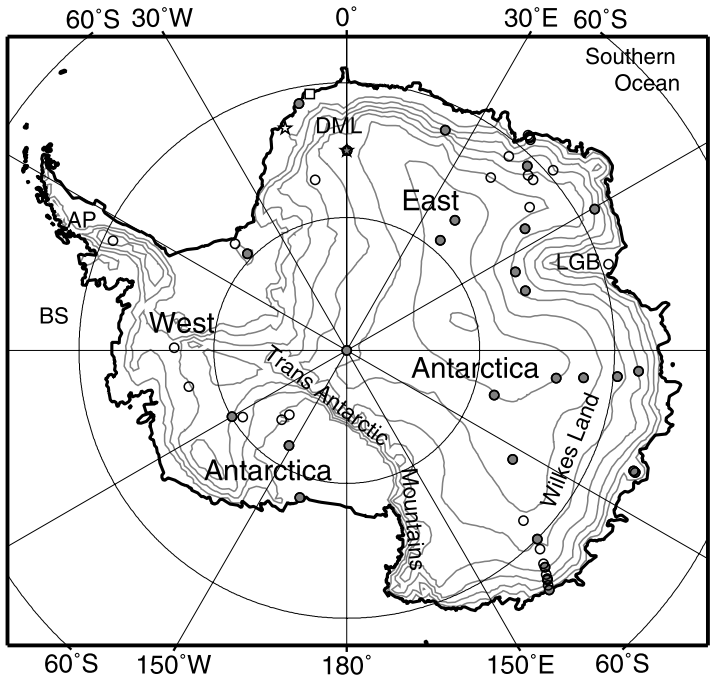

Figure 1. Map of Antarctica. Grey lines are 500 m elevation contours. The Antarctic Peninsula, Bellingshausen Sea, Dronning Maud Land and Lambert Glacier Basin are abbreviated to AP, BS, DML and LGB, respectively. Macquarie Island is outside this map. The square locates Neumayer station, and the left and right stars locate AWS 4 and AWS 9, respectively. Circles mark the locations of 10 m firn temperature observations. A solid grey circle marks a wind speed observation.

ture rise for the northern edge of the sea ice extend of up to 8 K in early winter. It also improves the agreement with temperature records from coastal stations.

4.1. Temperature and Wind

[28] For this study, the surface and upper air temperatures have been compared with deep snow temperature, (automatic) weather station data and radiosonde data from *Turner et al.* [2005], respectively. Observations locations are shown in Figure 1.

[29] In Figure 2a, the model simulated annual mean surface temperature for 1980 to 2004 is compared with observed 10 m firn temperatures. At this depth, the temperature closely resembles the climatological mean surface temperatures. The model has a 1.7 K cold bias compared to these observations, but is otherwise well capable to capture the 45 K wide range of annual mean surface temperatures in Antarctica (r = 0.996).

[30] Figure 2b compares the model simulated and observed mean annual upper air temperatures at the 10 stations that have at least ten complete years of observations. The model free atmosphere temperatures have a cool bias of up to 2 K, with a maximum deviation at 700 hPa. This bias is acceptable in comparison to the temperature range of 50 K that occurs through the troposphere (r = 0.999). This bias a winter and spring feature, i.e., from April to October; in summer and autumn a 1 K cool bias whole through the troposphere is found. The profile for Macquarie Island (158.9°E, 54.5°S) matches particularly well. This is because Macquarie Island is located in the lateral boundary zone of RACMO2/ANT in which the model is adjusted to the reanalysis data that are directly affected by these observations through data assimilation.

[31] Model simulated 10 m winds, presented in Figure 2c, also compare well with observations. The error bars of 1 m/s represent the typical uncertainty in the observations; for the model value they represent the uncertainty in representativeness, since many of the observational sites are located in complicated terrain and model values need to be interpolated. In line with the conclusions of *Reijmer et al.* [2005], the model slightly underestimates the range in wind speeds. Nevertheless, over the range of observations, the correlation between observed and model simulated wind speeds is very high (r = 0.91).

4.2. Surface Energy Budget

[32] The surface energy budget (SEB) is evaluated using SEB observations on two automatic weather stations (AWS) in Dronning Maud Land [*van den Broeke et al.*, 2005]. AWS 4 is situated on the Riiser-Larsen Ice Shelf (see Figure 1), 34 m asl, and AWS 9 is located near Kohnen base in the interior of East Antarctica, 2892 m asl. These observations have been chosen because they located in relatively homogenous terrain and they represent two different climate zones of Antarctica. The observations are made in the period from 1998 to 2001. Figure 3 shows the comparison of observed SEB (solid lines) with model results for the same time span (dotted lines). The results show that RACMO2/ANT reasonably captures the main characteristics of the SEB, but has some significant biases.

[33] Downwelling longwave radiation is underestimated by 10 to 30 W/m^2 throughout the year for both sites. *Guo et*

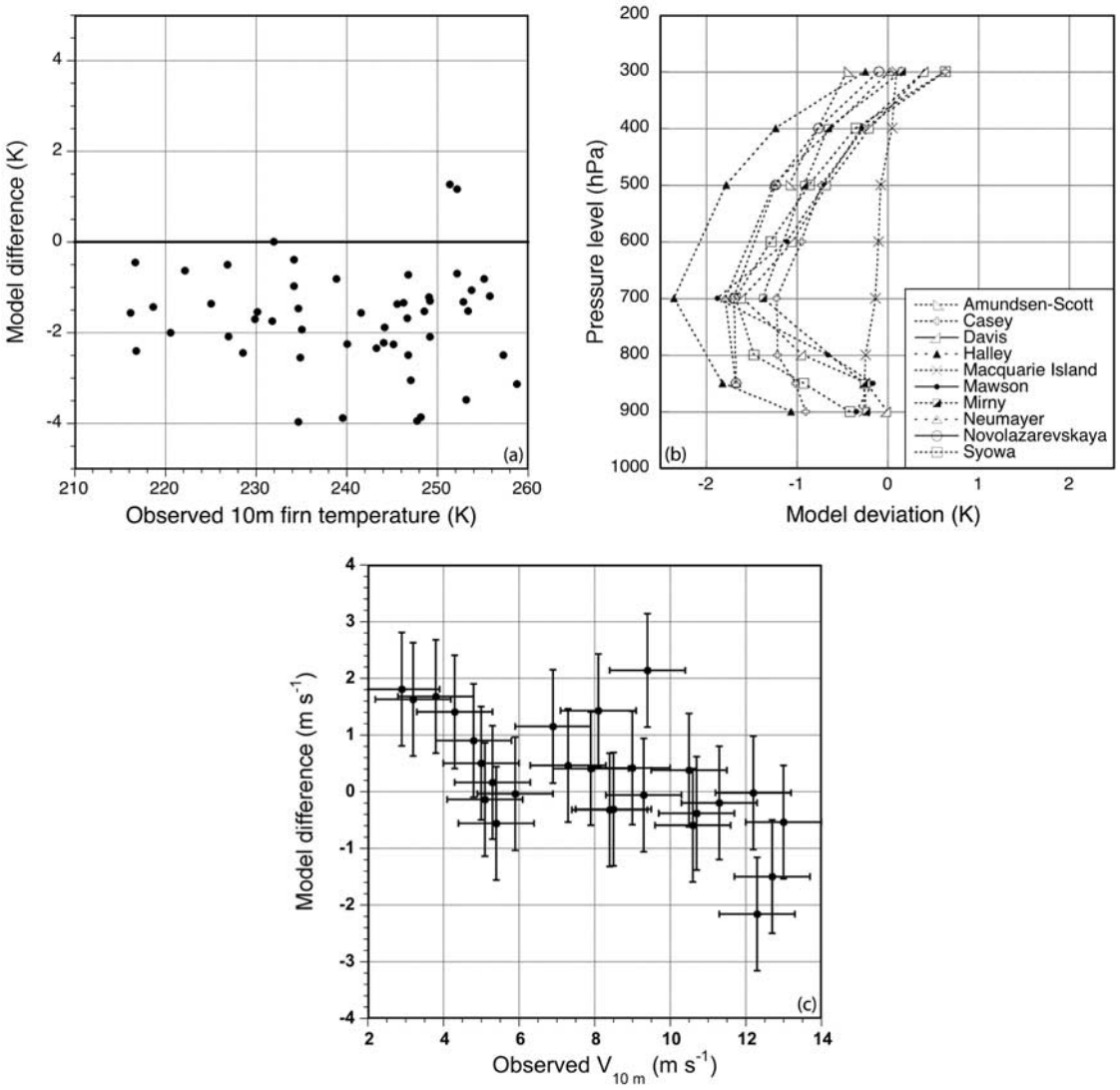

Figure 2. (a) Deviation of model simulated surface temperatures from observed 10 m firn temperatures. (b) Deviation of model simulated temperatures compared with radiosonde observations. The radiosonde data are from *Turner et al.* [2006]. (c) Deviation of model simulated 10 m winds compared to observed 10 m winds at (automatic) weather stations. Automatic weather station wind speeds were assumed to be representative for 3 m, and adjusted to 10 m, using $z_{0,m}$ = 1 mm and a neutral surface layer. Error bars give an impression of the uncertainty on the observations and model output.

al. [2003] found a similar underestimation and related it to an underestimation of humidity and cloud cover. The errors of both models show similarity, namely, a mid troposphere cool bias and underestimated precipitation on the plateau, which supports the assumption that the cloud parameterization contributes to the underestimation of downward *LW*. However, comparison of daily net *LW* against upgoing *LW* (not shown) indicates that also the LW radiation scheme contributes to the model flaw. AWS observations show that net *LW* is close to zero at cloudy days, while the maximum net *LW* emission for cloud free days is a function of the surface temperature [*van den Broeke et al.*, 2004, Figure 6]. For the location of AWS 9, RACMO2/ANT estimates not only too few cloudy days, but RACMO2/ANT also overestimates net *LW* emission by 20 W/m^2 for cloud free days, which is likely due to the radiation scheme.

[34] During winter, an excess downward *SHF* of 15 to 25 W/m^2 balances most of the excess *LW* cooling. During summer, excess *LW* cooling is partly compensated by overestimated downward *SHF* and *SW* absorption, and partly is introducing a cold surface temperature bias. If *SHF* is increased only in response to underestimated downwelling *LW*, the temperature bias should be largest during winter. The comparison with AWS data does not confirm this. So, the mixing scheme is too active, which introduces a compensating error, resulting in only a small bias in the surface temperature. The net *SW* surface absorption at AWS 9 matches well because overestimated *SW* transmissivity is balanced by a slightly underestimated albedo.

[35] How does this impact the atmospheric heat budget? The atmospheric heat budget and the SEB are closely

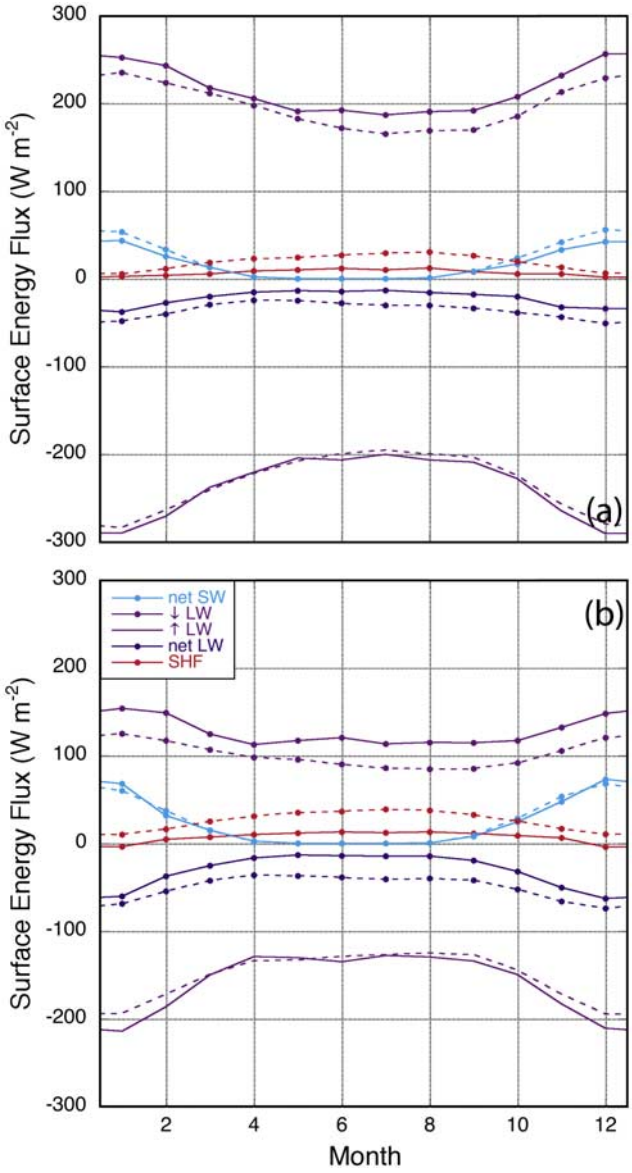

Figure 3. Comparison of surface energy fluxes from RACMO2/ANT (dotted lines) and observations (solid lines) at (a) AWS 4, situated at 72.75°S, 15.50°W, 34 m asl, and (b) AWS 9, situated at 75.00°S, 0.00°E, 2892 m asl. Fluxes are positive when pointing toward the surface.

related, because downwelling *LW* and *SHF* are largely from the ABL. The error margin shows that, although primary variables like temperature and wind are well simulated, *LW* and *SHF* parameterizations still need to be further improved for Antarctic conditions. However, we do not expect improved parameterizations to dramatically alter the results presented in this paper.

5. Results

5.1. Binning Procedure

[36] Vertical profiles of the heat budget terms have been binned in500 m surface elevation intervals (Table 2) for the sector between 30°W and 150°E. This sector of East Antarctica excludes the Transantarctic Mountains and has a rather uniform topography, making binning meaningful. Over the coastal seas, binning has been done in 200 km distance intervals, excluding the lateral boundary zone. The heat budget terms are presented as temperature tendencies in K day^{-1}.

[37] Over the ice sheet, wind vectors were rotated to obtain cross-slope and alongslope directions for u and v, respectively (Figure 4). Over sea, u and v follow the geographical coordinate system. For the analysis of the strength of the near-surface temperature deficit, a background temperature profile (θ_0) was extrapolated from the free atmosphere vertical potential temperature gradient toward the surface. Using this background profile, large-scale wind (u_{lsc}, v_{lsc}) profiles can be obtained assuming thermal wind balance with θ_0, namely

$$\frac{\partial u_{lsc}}{\partial \ln p} = +\frac{R_d}{f}\left(\frac{p}{p_0}\right)^{\frac{R_d}{c_p}}\frac{\partial \theta_0}{\partial y}$$
$$\frac{\partial v_{lsc}}{\partial \ln p} = -\frac{R_d}{f}\left(\frac{p}{p_0}\right)^{\frac{R_d}{c_p}}\frac{\partial \theta_0}{\partial x}, \quad (5)$$

in which p_0 = 1013.25 hPa. θ_0, u_{lsc} and v_{lsc} have been calculated with monthly means.

5.2. Climatological Setting

[38] Figures 5a and 5b show the potential temperature (colors) and cross-slope wind profiles (contours) for winter (JJA) and summer (DJ), respectively, averaged for 1980 to 2004. Figures 5c and 5d enlarge Figures 5a and 5b near the surface, respectively. Vertical (colors) and alongslope (contours) wind speeds are shown in Figures 5e and 5f. In all these figures, the dotted lines indicate two η-layers for orientation and interpretation of the advection terms.

[39] A prominent feature of the winter lower atmosphere over East Antarctica is the strong near-surface temperature deficit (Figures 5a and 5c). The potential temperature near the surface in the interior decreases below 250 K while the free atmosphere is close to 280 K (Figure 5c). In the free atmosphere the horizontal temperature gradient is large, typically 12 K/2000 km, forcing an eastward thermal wind of 2 m/(s km). Thus the winds rotate from upper air westerlies to near-surface easterlies (Figure 5a). The katabatic enhancement in the ABL is clearly visible as an increased easterly wind. The wind preserves an along slope component in a shallow layer near the surface, due to friction (Figure 5e). Above the ABL, along slope winds are small and directed inland except in the far interior. Figure 5e shows large-scale subsidence ($w < 0$) above the ice sheet and upward motion ($w > 0$) over the adjacent ocean. The maximum in vertical velocity at the margin is due to the accumulation of cold air. During summer, the temperature gradients are smaller, and therefore the horizontal and vertical wind speeds are lower throughout the troposphere.

[40] In Figures 5a and 5b, a discontinuity appears near the margin of Antarctica. This is a feature introduced by the binning procedure. The low coastal bin (0–150 m asl) contains ice shelf grid points, and therefore is the only bin in which the grid points are not evenly distributed along the coast of East Antarctica; ice shelves are located in coastal

Table 2. Characteristics of the Bins, Which Contain the Data From Grid Points Between 30°W and 150°E[a]

Bin Number	Elevation/DTC	Bin Name	Area, % of Total	Mean DTC, km
1	>3750 m asl	high interior	1.7	−1245
2	3250–3750 m asl	middle interior	10.8	−956
3	2750–3250 m asl	low interior	13.9	−757
4	2250–2750 m asl	high escarpment	11.1	−544
5	1750–2250 m asl	middle escarpment	5.6	−336
6	1250–1750 m asl	low escarpment	4.1	−212
7	750–1250 m asl	high coastal	3.1	−134
8	150–750 m asl	middle coastal	2.7	−76
9	0–150 m asl	low coastal	2.3	−40
10	0–200 km	coastal sea	10.2	116
11	200–400 km		11.3	306
12	400–600 km		10.4	500
13	600–800 km		7.7	693
14	800–1000 km		5.2	893

[a]DTC is the distance to the nearest coastal grid point.

Dronning Maud Land and in the Lambert Glacier Basin. Both locations have lower temperatures and weaker westerlies than the coastal average.

[41] In Figures 5e and 5f, an irregularity is visible in the vertical wind speed at some height above the coastal zone. This is related to diffusion, which damps small-scale variations along η-levels. However, as η-levels partly follow the surface, an η-level contains elevation related temperature variations. Although the diffusion scheme corrects for the elevation, some persistent energy transport is nevertheless introduced in regions of steep topographic gradients. This transport is counterbalanced by advection, thereby introducing a secondary circulation. This circulation is negligible on synoptic timescales as is its effect on climatological means of temperature and horizontal wind. However, it does have a significant influence on the average vertical wind speed, which is a diagnostic parameter in a hydrostatic model. As a result, the advective heat budget terms must be treated with caution in the higher atmosphere over the coastal zone of East Antarctica.

5.3. Winter Heat Budgets

[42] In this section, the heat budgets of East Antarctica for winter, i.e., June, July and August, are presented for four representative bins: the interior, escarpment, coastal zone and coastal seas (Table 2).

5.3.1. Interior

[43] Figure 6 shows profiles for the middle interior bin, which is representative for all three interior bins. This bin has a surface temperature deficit of 27 K (Figure 6a). The temperature deficit layer is shallow; at 500 m above the surface the temperature deficit is reduced to only 3 K. The large-scale circulation is anticyclonic without a significant along slope component. In the ABL momentum budget, a balance is struck between the large-scale and katabatic pressure gradient force, turbulent surface drag and coriolis deflection [*van den Broeke et al.*, 2002]. Close to the surface, the along slope component matches the cross-slope component in size. At the top of the ABL, the wind is directed purely along the elevation contours.

[44] The vertical profiles of turbulent sensible heat flux (*SHF*), net longwave radiation (*LW*), and convection heat flux (*CHF*) are shown in Figure 6b. Positive values indicate energy transport toward the surface. The flux of shortwave radiation is not included here in the absence of sunlight during winter. The surface net emission of *LW* is 36 W/m^2, one third of the total emission at the top of the atmosphere. At the surface, all the lost energy in the form of longwave radiation is balanced by *SHF*, heating the surface and cooling the ABL. The flux of energy related to convection is negligible, as is expected in the very cold and stable ABL during the polar winter night.

[45] The vertical divergence of the fluxes shown in Figure 6b determines the temperature tendencies in Figure 6c. In the ABL, *SHD* is the dominant cooling term. Higher up, cooling by longwave radiation is dominant. Near the surface, the cooling by *LWD* nearly vanishes, this cold layer is almost in radiative balance. The very stable and dry conditions over the plateau cause *CHD* and *Q* to be insignificant. Therefore all heat that is lost by *LWD* and *SHD* must be supplied by advection. Over the whole column *AdvV* is the main source of heating, although in the lower ABL *AdvH* is a significant heating term too, caused by the strong decrease in the depth of the temperature deficit layer toward the interior in combination with a significant along slope wind (Figure 5c). Note that on long

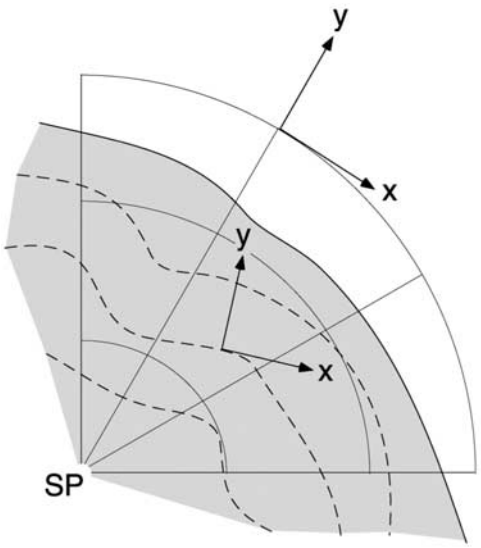

Figure 4. Orientation of the cross- (x) and along-slope (y) coordinates over the ice sheet. The dashed lines are schematic height contours. Over the ocean, ordinary S-N and W-E coordinates are used.

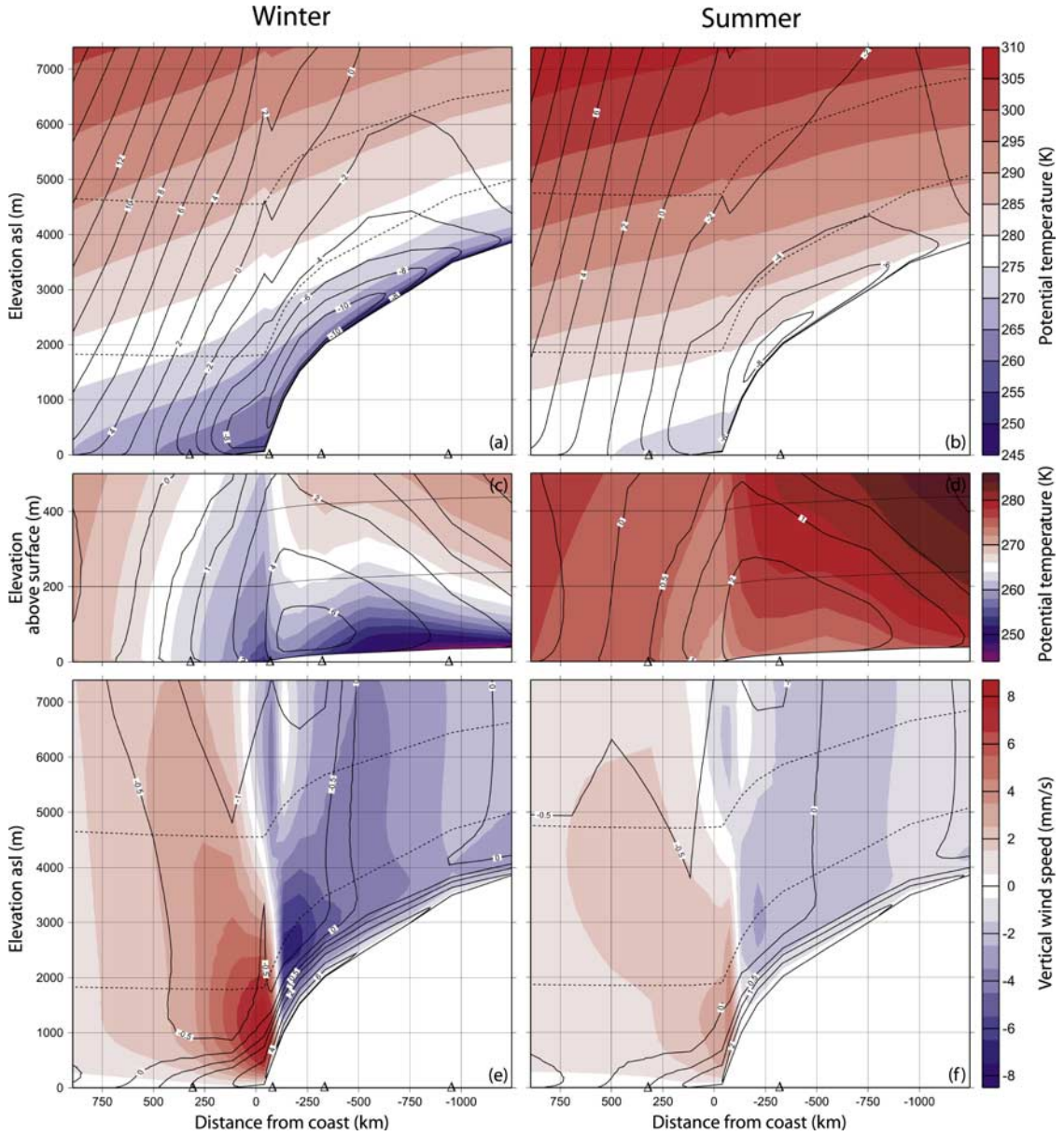

Figure 5. Bin average potential temperature (colors) with contours of cross-slope wind speed (m s^{-1}) for (a) winter and (b) December and January, i.e., summer. (c and d) Magnifications of the near surface potential temperature and alongslope wind (m s^{-1}) for winter and summer, respectively. The surface elevation is schematically included for orientation. (e and f) Bin average of vertical velocity (colors, mm s^{-1}) and contours of alongslope wind speed (m s^{-1}) for winter and summer, respectively. In Figures 5a, 5b, 5e and 5f, dashed lines show η-levels for orientation. Triangles mark the positions of the presented profiles.

timescales *AdvH* is insignificant in the free atmosphere heat budget, despite the fact that synoptic-scale systems like depressions do have a short-term impact on the temperatures through the whole troposphere [*van As et al.*, 2005].

[46] As concluded in section 3.2, *SHD* and *LWD* are prone to significant model uncertainties. For *SHD* this implies that the cooling strength and/or layer depth is overestimated, but because of its overwhelming modeled strength, *SHD* nonetheless is a dominant heat budget term in the ABL. In return, *LWD* cooling is somewhat underestimated, but it cannot be determined whether this additional cooling is spread out through the whole atmosphere or enhances the cooling maximum in the ABL.

5.3.2. Escarpment

[47] The escarpment is characterized by increasing surface slopes. Furthermore, the plateau acts as a reservoir of cold air for the escarpment. Profiles for the middle escarpment, 1750 to 2250 m asl, are presented in Figure 7. Figure 7a shows that the katabatic winds are much stronger than in the interior, resulting in stronger vertical mixing and a thicker temperature deficit layer. The surface temperature deficit of 18 K is still considerable, and decreases more gradually with height than in the interior. Furthermore, the free atmosphere is about 5 K warmer than in the middle interior bin. Owing to increased baroclinicity, the prevailing winds change from easterly to westerly at a lower elevation.

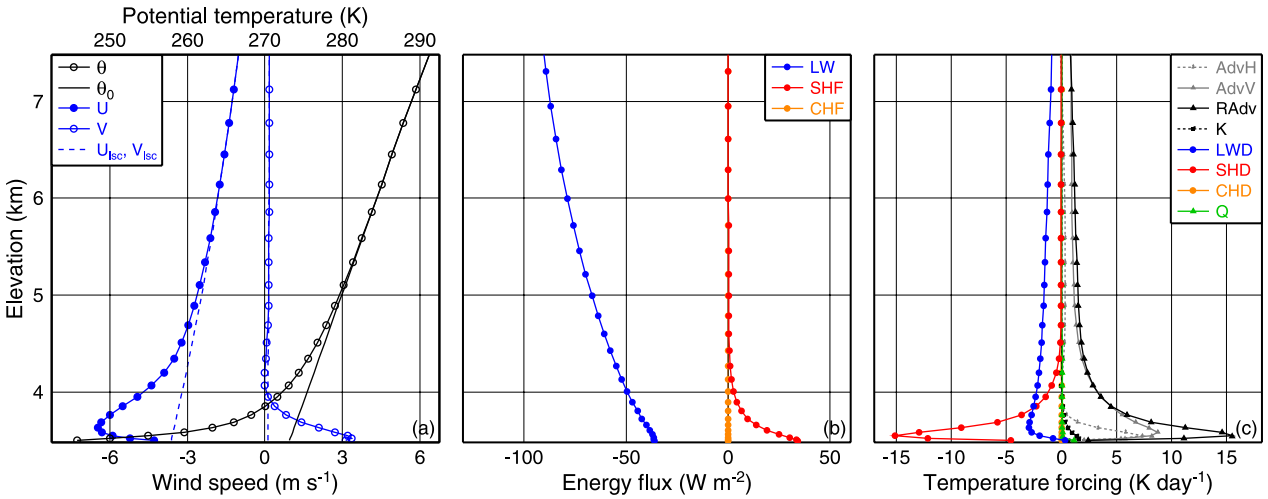

Figure 6. Winter vertical profiles for the middle interior of (a) potential temperature (θ), background potential temperature (θ_0), cross-slope (U) and alongslope (V) wind, and their large-scale component (U_{lsc}, V_{lsc}); (b) *LW*, *SHF* and *CHF*; and (c) the heat budget terms.

Above 2800 m asl, the winds also have a significant upslope component.

[48] The vertical profiles of the energy fluxes (Figure 7b) are qualitatively similar to the middle interior. Again the surface net longwave emission is balanced by *SHF*, while *CHF* is negligible.

[49] The katabatic nature of the ABL has a strong impact on the heat budget, as presented in Figure 7c. The increased depth of the ABL compared to the interior enables turbulent mixing to extract heat from a deeper layer, and therefore the maximum cooling rate by *SHD* is less than half of that in the interior. Above the ABL, *LWD* remains the dominant cooling term, while subsidence (*AdvV*) is the dominant source of heat.

[50] Contrary to the interior, *AdvH* is significant, because of a significant alongslope wind in combination with horizontal temperature gradients (Figures 5c and 7a). In the lowest 150 m of the ABL, *AdvH* cools the air by along slope advection of cold near-surface air from the interior. Surface friction maintains the along slope wind component, so its effect decreases quickly when moving away from the surface. Cold air descends the escarpment thus faster near the surface than in the upper ABL. The advection of this shallow, cold layer reduces the vertical temperature difference with the colder surface, but enhances the vertical temperature difference with the warmer upper ABL. As a result, the *SHF* at the top of the cold layer, which is further increased by the strong wind shear in the upper ABL, exceeds the *SHF* at the surface (Figure 7b), resulting in a reversal of the vertical *SHF* gradient and a heating of a shallow layer by *SHD* (Figure 7c), from now on referred to as SHF inversion layer. Analysis of the control year showed that about half of *K* can be attributed to *SHD*, which implies that *SHF* inversion might be even stronger.

[51] Owing to the deepening of the ABL, the temperature gradient along η-levels changes sign in the middle ABL,

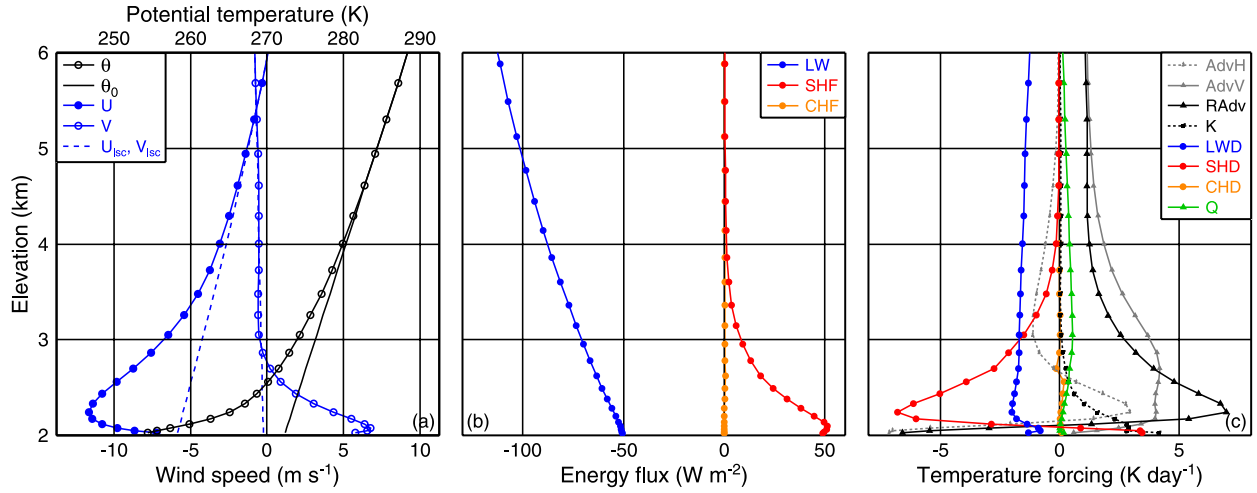

Figure 7. Winter vertical profiles for the middle escarpment of (a) potential temperature (θ), background potential temperature (θ_0), cross-slope (U) and alongslope (V) wind, and their large-scale component (U_{lsc}, V_{lsc}); (b) *LW*, *SHF* and *CHF*; and (c) the heat budget terms.

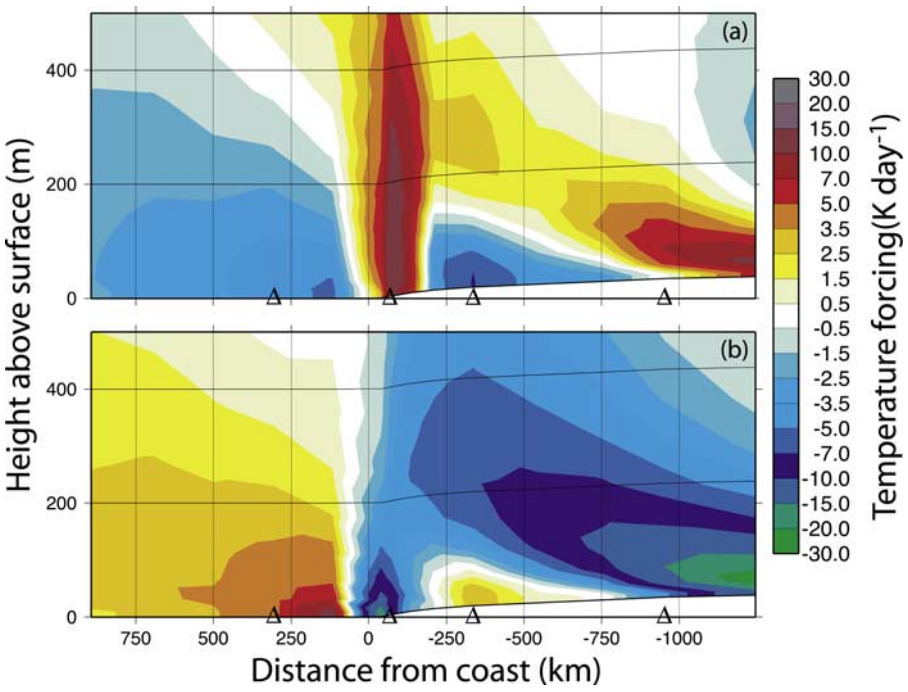

Figure 8. Bin winter averages of (a) *AdvH* and (b) *SHD*. The surface elevation is schematically included for orientation. Triangles mark the locations of the presented bins.

and *AdvH* also becomes a heating term between 150 and 600 m above the surface. Above that level, the alongslope wind component becomes directed upslope (Figure 7a) so that *AdvH* changes sign once more back to cooling. Finally, heating by condensation, represented by *Q*, gains importance while approaching the coast, but is still small.

[52] The sign reversal of *SHD* from cooling to heating in a shallow near-surface layer is most pronounced in this transitional bin (~336 km inland) between interior and coast (Figure 8), but occurs throughout the whole escarpment (200 to 600 km inland). A preliminary analysis of the spatial occurrence of this *SHF* inversion layer indicates that it appears in places where the katabatic outflow has a long path over homogeneous terrain. For example, the whole margin of Wilkes Land exhibits a thick budget reversal layer, but *SHF* inversion layers rarely occur in Dronning Maud Land. The spatial variability of the ABL heat budget is the topic of a forthcoming paper.

[53] We consider the *SHF* inversion layer as a realistic feature. The model simulated near-surface air potential temperature increases toward the coast in the escarpment (Figure 5c) agrees with observations [*van den Broeke et al.*, 1999]. Turbulent redistribution of heat in the ABL is the only mechanism that can provide enough heat to establish this temperature increase. *AdvV*, for example, quickly decreases in magnitude in the lowest 100 m because the vertical wind becomes zero at the surface.

5.3.3. Coastal Zone

[54] In Figure 9, profiles for the middle coastal bin (150–750 m asl) are shown. The elevation interval has been adjusted, so that the low coastal bin contains mainly grid points on ice shelves (0–150 m asl) and the middle coastal bins mainly grid points on grounded ice. The coastal margin is under oceanic influence, but still has similarities with more inland profiles. For example, the temperature deficit (Figure 9a) is strongest near the surface, but is also more vertically extensive, reaching up to about 2500 m asl, because of piling up of cold air seaward of the ice sheet on the ice shelves and sea ice. The wind still has a katabatic component and rotates in a 1500 m deep layer from its surface direction to cross-slope in the free atmosphere. The cross-slope wind reversal from east to west is located at 4300 m for this bin. The large-scale upslope wind is nearly equal to that in the middle escarpment, about −1 m/s.

[55] The vertical profiles of the energy fluxes in the mid coastal bin (Figure 9b) again show that longwave cooling at the surface is compensated mainly by *SHF*. *SHD* (Figure 9c) is nonzero over a very deep layer and extracts energy from the air up to 2500 m asl, with the highest cooling rates near the surface. At the foot of the ice sheet, in the absence of katabatic forcing, the cold air from the ice sheet accumulates. The accumulation of air leads to upward motion and a negative *AdvV*, which cools the air together with *LWD* and *SHD*. As a result, the ABL potential temperature is lower than in the escarpment (Figure 5c), which turns *AdvH* into a significant heating term in the lowest 1,5 km, which is also visible in Figure 8a.

[56] In the cloud layer, between 1 and 5 km asl, heat release by water phase transitions (*Q*) is an important heat source. Diffusion (*K*), included in the model dynamics for numerical stability, is a heating term in the lower free atmosphere for the low and middle coastal bins, and a cooling term in this layer for the high coastal and low escarpment bins. No physical process can be directly linked to this model heat transport.

5.3.4. Coastal Seas

[57] The eleventh bin represents the seas surrounding East Antarctica from 200 to 400 km offshore (Figure 10).

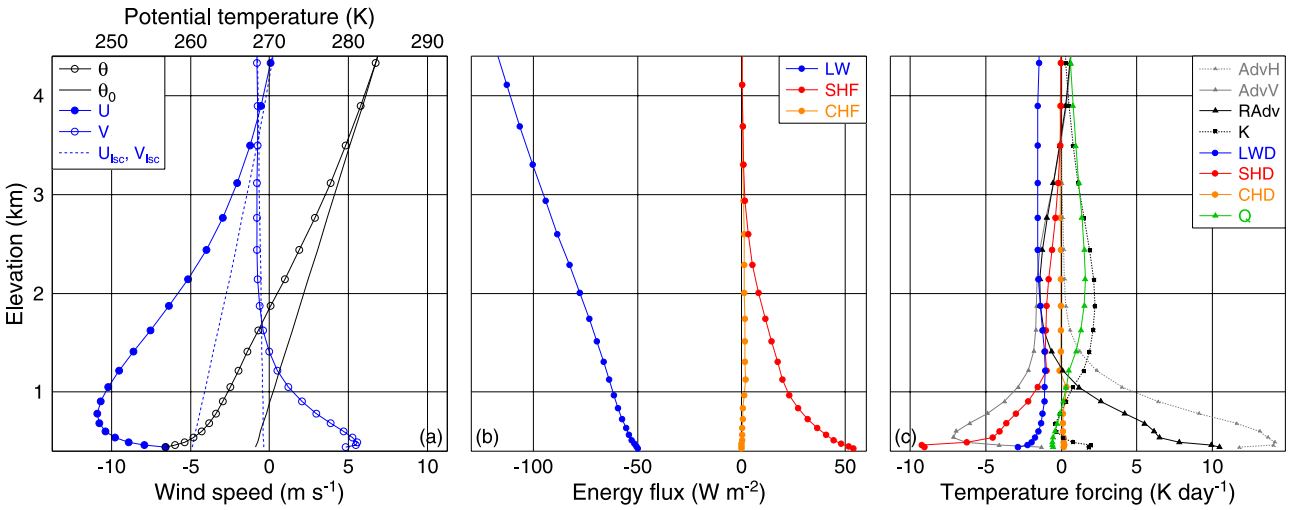

Figure 9. Winter vertical profiles for the middle coastal bin of (a) potential temperature (θ), background potential temperature (θ_0), cross-slope (U) and alongslope (V) wind, and their large-scale component (U_{lsc}, V_{lsc}); (b) *LW*, *SHF* and *CHF*; and (c) the heat budget terms.

The wintertime sea ice fraction for this bin is on average 0.79. The profile of the potential temperature (Figure 10a) reveals a 1500 m thick layer of cold air, which is made possible by the winter sea ice. Noncontinuous sea ice, however, allows a significant ocean-atmosphere heat exchange, therefore a strong surface inversion does not build up. Winds are primarily large-scale driven. The meridional flow is southerly in the lowest 500 m and northerly above. The low-level southerly flow is forced by a combination of friction and cold air spreading out from the continental margin [*van den Broeke et al.*, 2002]. The zonal circulation is easterly in the lower atmosphere and changes to westerly above 1.5 km. As shown in Figure 5a, from 500 km offshore northward, the flow is westerly throughout the atmosphere.

[58] The vertical profiles of the energy fluxes for this bin are shown in Figure 10b. This area has a high cloud amount, which reduces the net emission of *LW*-radiation at the surface compared to the ice sheet. The open water fraction is a source of turbulent heat, i.e., a negative *SHF*. In winter, the flux of *SW* is nonzero at this latitude, but still insignificant.

[59] The heat budget for this bin is shown in Figure 10c. Compared to bins over the ice sheet, the magnitudes are relatively small, because, unlike the ice sheet, the sea surface does not extract large amounts of heat from the atmosphere. As a result horizontal and vertical temperature gradients are smaller. *AdvH*, related to the outflow of cold air, is the dominant cooling term in the lowest 500 m, while *SHD* is the largest heating term. This heat is supplied by the upper part of the ABL and the ice-free sea surface part. Analysis shows that *AdvH* and *SHD* budgets are larger over largely ice free locations compared to locations with almost full sea ice cover. Convection transports heat from the higher ABL downward, since ascents are saturated-adiabatic and descents are dry-adiabatic. Q is negative near the surface because of melt and evaporation of falling snow. The

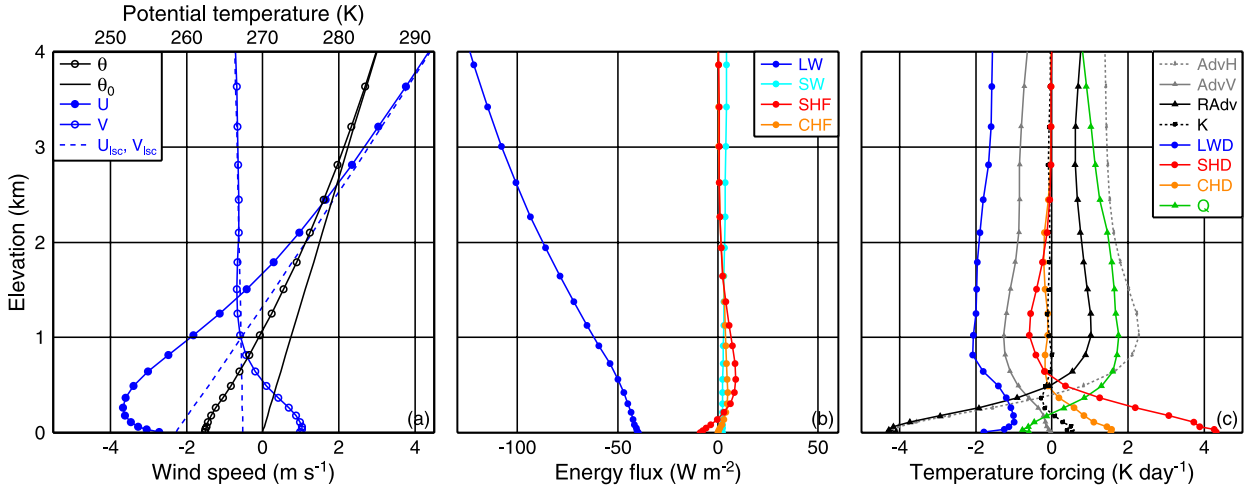

Figure 10. Winter vertical profiles for the second sea bin 200 to 400 km offshore of (a) potential temperature (θ), background potential temperature (θ_0), cross-slope (U) and alongslope (V) wind, and their large-scale component (U_{lsc}, V_{lsc}); (b) *LW*, *SHF* and *CHF*; and (c) the heat budget terms.

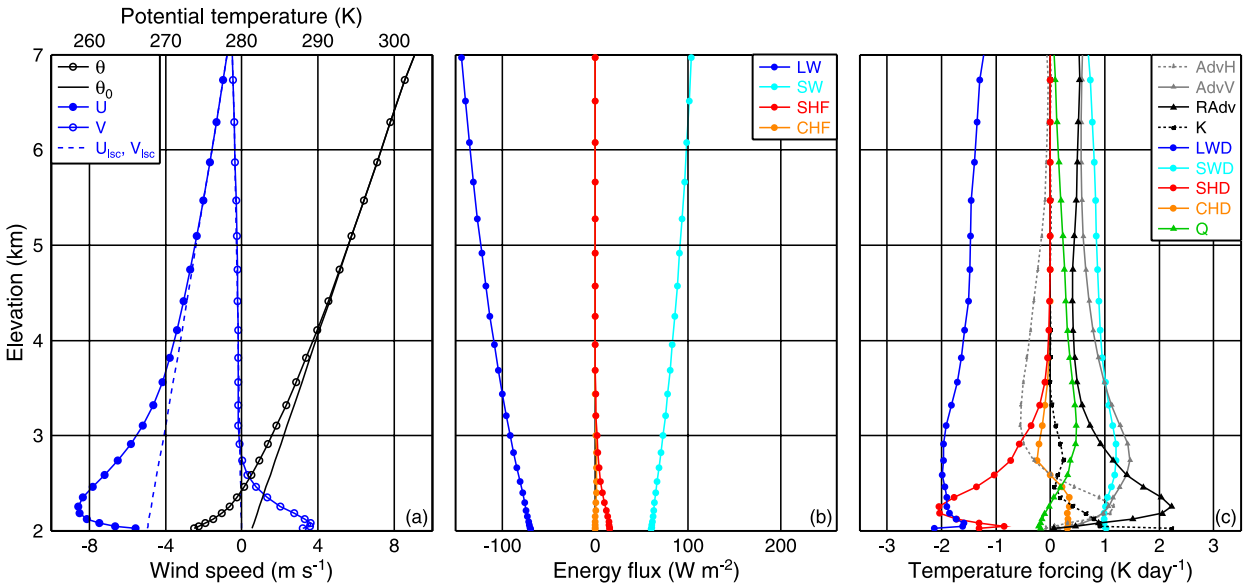

Figure 11. Summer vertical profiles for the middle escarpment of (a) potential temperature (θ), background potential temperature (θ_0), cross-slope (U) and alongslope (V) wind, and their large-scale component (U_{lsc}, V_{lsc}); (b) *LW*, *SW*, *SHF* and *CHF*; and (c) the heat budget terms.

nonzero values of *K* in this bin do not represent diffusional transport but is related to the mixing in clouds, which have not properly been diagnosed during the model integration (see section 2.2).

[60] Above the ABL, *LWD* and *AdvV* are the most important cooling terms. Both have a maximum in the cloud layer, at about 1000 m. Below the clouds in the ABL, the net longwave emission is reduced. Above the ABL, the heat losses are balanced by *CHF* and *AdvH*. This balance reflects the influence of cyclones in the offshore Antarctic heat budget.

5.4. Summer Heat Budgets

[61] In the Antarctic interior, December and January are the only summer months, because insolation already decreases significantly in February. Therefore averages for these 2 months are considered representative for the summer period, starting in December 1979 and ending in January 2004.

5.4.1. Ice Sheet

[62] The summer heat budget profiles for the middle escarpment (1750–2250 m asl) (Figure 11c) are found representative for most ice sheet bins in East Antarctica.

[63] The solar insolation is the principal difference between summer and winter. In summer, *SW* heating nearly balances the net *LW* cooling at the surface (Figure 11b). As a result, vertical potential temperature gradients are small and turbulent mixing extracts less heat from the ABL. The temperature deficit is strongly reduced and katabatic winds are weaker (Figure 11a). Both in the interior and the escarpment, the katabatic and large-scale forcing are of equal importance in the momentum budget of the ABL. The wind in the coastal zone of the ice sheet is even dominated by the large-scale forcing [*van den Broeke et al.*, 2002].

[64] The summer insolation resulting in a weaker katabatic nature of the ABL reduces nearly all terms in the heat budget (Figure 11c). This reduction, up to a factor five, is strongest in the interior (not shown). With the exception of the *SHF* inversion layer, which disappears in summer, the shape of the profiles is qualitatively similar to winter (compare to Figure 7c). The magnitudes of *LWD* and *Q* are similar to the winter profiles. The effect of clouds is especially important with respect to *SWD* at the same elevation. Evaporation of falling snow cools the lower ABL with a rate of up to 1 K per day of the coastal zone (not shown). Absorption of shortwave radiation *SWD* provides about half of the energy lost through longwave cooling. As a result of weaker θ gradients and weaker winds, *Adv* + *K* is halved in summer compared to winter, whereby the ratios between *AdvH*, *AdvV* and *K* do not change significantly.

[65] Finally, *CHF* is significantly different from zero in the ice sheet summertime ABL. The ECMWF mass flux scheme, which parameterizes convection, is activated if the ABL becomes near neutral during daytime. Since convection is bound by the top of the ABL, the extent of the nonzero *CHF*-layer indicates the maximum depth of the daytime ABL. In the interior (not shown) this is about 600 m; in the escarpment and coastal zone it is about 1400 m. These numbers are generally higher than values reported by observations [*Mastrantonio et al.*, 1999; *van As and van den Broeke*, 2006], indicating that the ECMWF mass flux scheme is too active under these conditions.

5.4.2. Coastal Seas

[66] Figure 12 shows profiles for bin 11, 200 to 400 km offshore. These profiles are representative for the seas around East Antarctica. In summer, the effect of outflow of cold air from the continent on the temperature is small. A weak but vertically extensive potential temperature deficit (Figure 12a) is found for this bin. Diabatically forced lift is the likely cause of the increased stability of the lower atmosphere. The wind profile is primarily determined by the large-scale circulation.

[67] The flux profiles over the sea (Figure 12b) are significantly different from those over land. Clouds strongly

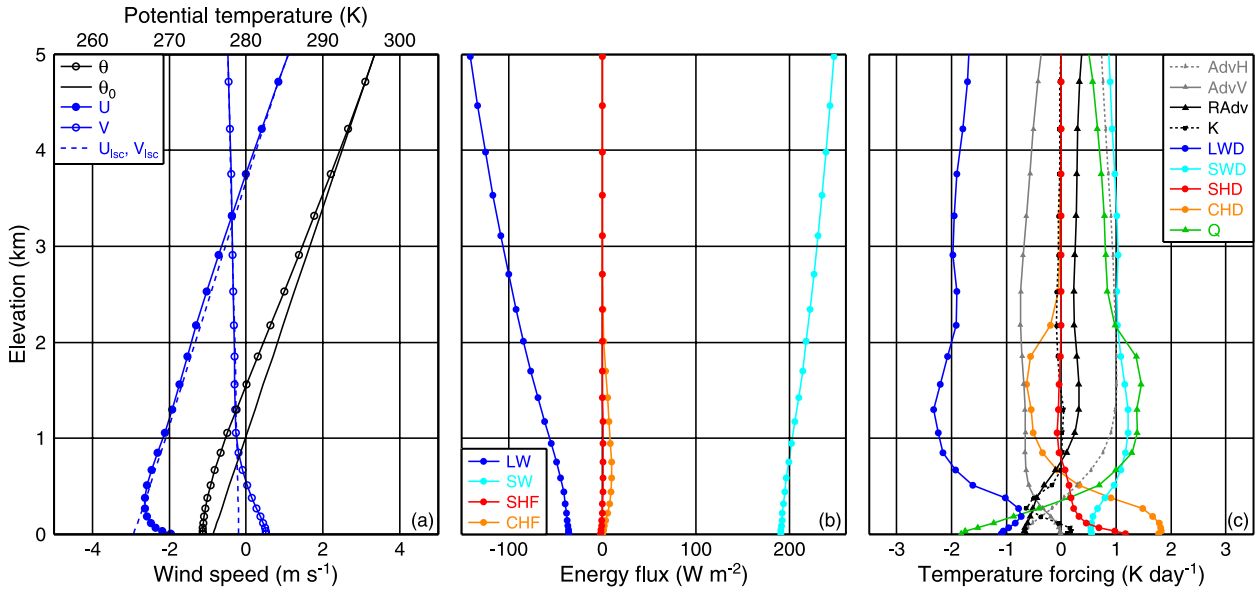

Figure 12. Summer vertical profiles for the second sea bin 200 to 400 km offshore of (a) potential temperature (θ), background potential temperature (θ_0), cross-slope (U) and alongslope (V) wind, and their large-scale component (U_{lsc}, V_{lsc}); (b) *LW*, *SW*, *SHF* and *CHF*; and (c) the heat budget terms.

reduce the net *LW* emission at the surface, and the low ocean albedo enlarges the net surface *SW* insolation. *CHF* is larger than *SHF*, but both are small compared to the radiative fluxes.

[68] Three layers can be distinguished in (Figure 12c). The uppermost layer extends from 2 km upward. This layer is not part of the ABL, since *SHD* and *CHD* are both zero. Cyclonic activity is evident from the large-scale upward motion (negative *AdvV*), the enhanced condensation, and the increased *LWD* and *SWD* due to the higher cloud amounts compared to the coastal bin (not shown). Although *Q* and *SWD* are significant heating terms, the free atmosphere experiences a net sink of heat, hence *RAdv* is positive.

[69] The middle layer extends from about 500 m up to 2 km. Here, the additional effect of ABL clouds (stratocumulus, shallow clouds) can be noticed. Convection itself removes some heat from the cloud layer, but that is compensated by additional condensation (*Q*). The profiles of *LWD* and *SWD* show that cloud tops experience strong longwave cooling and shortwave heating, while inside the cloud, the radiation budgets are reduced.

[70] The lowest 500 m represents the subcloud layer. Net *LWD* and *SWD* are reduced by the clouds. The downdrafts of the stratocumulus through *CHF*, absorption of sunlight (*SWD*) and the sensible heat uptake from the sea surface (*SHD*) are the dominant heating terms. Melt of snow and evaporation of precipitation have an important cooling effect. The nonzero value of *K* represents subcloud turbulent mixing and not numerical diffusion (see section 2.2). In this layer, *AdvH* is negative because of weak remaining cold air outflow (Figure 12a). Further offshore, this term becomes zero (not shown).

6. Conclusions

[71] A detailed analysis of the model simulated heat budget of the lower atmosphere over East Antarctica is presented, averaged in nine surface elevation bins over the ice sheet and five distance bins over the coastal seas.

[72] Direct observations of the heat budget are not available, so the results shown here can only be indirectly evaluated by comparing model simulated and observed temperatures and surface energy fluxes at the surface. Over the ice sheet the model tends to overestimate the surface *SHF* and underestimate the downwelling *LW* flux. Possible reasons are an overactive mixing scheme and an underestimated cloud cover or atmospheric longwave emissivity. These errors counterbalance, so the surface temperature is found to match the observations well.

[73] The wintertime Antarctic surface is cooled by net longwave emission, which is balanced by a sensible heat flux from the lower atmosphere. As a result, vertical turbulent mixing is the dominant heat loss in the ABL, balanced by vertical and horizontal heat advection. In the interior, advection is mostly vertical through subsidence; near the coast, it becomes predominantly horizontal. In the escarpment, a shallow (<100 m) near surface layer is found where turbulent mixing acts as a heat source, while horizontal advection cools. Above the ice sheet ABL, a balance is struck between longwave cooling and heating by subsidence. Heating by condensation is only important in the free atmosphere of the coastal zone.

[74] In summer, the surface is in near-radiative balance, so that the horizontal and vertical potential temperature gradients are strongly reduced over the ice sheet and the coastal seas. As a result, cooling by turbulent mixing and advective heating are much smaller than in winter. Throughout the atmosphere, absorption of shortwave radiation is a heating term, but compensates only half of the longwave cooling. Above the ABL, advection is weaker than in winter, while condensational heating remains largely unchanged.

[75] Apart from insight in the dynamics of the atmosphere, analysis of the heat budget elucidates the possible

impact of inaccuracies of parameterizations on the model climate. The ECMWF parameterizations of clouds, longwave radiation and turbulent mixing still have flaws in the cold and stable atmosphere over the East Antarctic ice sheet.

[76] In the near future, we plan to explore in more detail the regional and temporal variability of the ABL heat budget. Special attention will be paid to the interaction between topography, katabatic wind and heat advection.

References

Andreas, E. L. (1987), A theory for the scalar roughness and the scalar transfer coefficients over snow and sea ice, *Boundary Layer Meteorol.*, *38*, 159–184.

Bromwich, D. H., and R. L. Fogt (2004), Strong trends in the skill of the ERA-40 and NCEP-NCAR reanalyses in the high and midlatitudes of the Southern Hemisphere, 1958–2001, *J. Clim.*, *17*, 4603–4619.

Brost, R. A., and J. C. Wyngaard (1978), A model study of the stably stratified planetary boundary layer, *J. Atmos. Sci.*, *35*, 1427–1440.

Cerni, T. A., and T. R. Parish (1984), A radiative model of the stable nocturnal boundary layer with application to the polar night, *J. Clim. Appl. Meteorol.*, *23*, 1563–1572.

Connolley, W. M. (1996), The Antarctic temperature inversion, *Int. J. Climatol.*, *16*, 1333–1342.

Guo, Z., D. H. Bromwich, and J. J. Cassano (2003), Evaluation of polar MM5 simulations of Antarctic atmospheric circulation, *Mon. Weather Rev.*, *131*, 384–411.

Holton, J. R. (1992), *An Introduction to Dynamic Meteorology*, *Int. Geophys. Ser.*, vol. 48, 3rd ed., Elsevier, New York.

Intergovernmental Panel on Climate Change (2001), Climate Change 2001: The Scientific Basis—Contribution of Working Group 1 to the Third Assessment Report of the Intergovernmental Panel on Climate Change, Cambridge Univ. Press, New York.

King, J. C., W. M. Connolley, and S. H. Derbyshire (2001), Sensitivity of modelled Antarctic climate to surface and boundary-layer flux parameterizations, *Q. J. R. Meteorol. Soc.*, *127*, 779–794.

Lenderink, G., B. van den Hurk, E. van Meijgaard, A. van Ulden, and H. Cuijpers (2003), Simulation of present-day climate in RACMO2: First results and model developments, *Tech. Rep. TR-252*, R. Dutch Meteorol. Inst., Utrecht, Netherlands.

Mastrantonio, G., V. Malvestuto, S. A. Argentini, T. Georgiadis, and A. Viola (1999), Evidence of a convective boundary layer developing on the Antarctic Plateau during the summer, *Meteorol. Atmos. Phys.*, *71*, 127–132.

Parish, T. R., and D. H. Bromwich (1987), The surface windfield over the Antarctic ice sheets, *Nature*, *328*, 51–54.

Parish, T. R., and J. J. Cassano (2003), Diagnosis of the katabatic wind influence on the wintertime Antarctic surface wind field from numerical simulations, *Mon. Weather Rev.*, *131*, 1128–1139.

Reijmer, C., E. van Meijgaard, and M. van den Broeke (2004), Numerical studies with a regional atmospheric climate model based on changes in the roughness length for momentum and heat over Antarctica, *Boundary Layer Meteorol.*, *111*(2), 313–337.

Reijmer, C. H., E. van Meijgaard, and M. R. van den Broeke (2005), Evaluation of temperature and wind over Antarctica in a Regional Atmospheric Climate Model using 1 year of automatic weather station data and upper air observations, *J. Geophys. Res.*, *110*, D04103, doi:10.1029/2004JD005234.

Renfrew, I. A. (2004), The dynamics of idealized katabatic flow over a moderate slope and ice shelf, *Q. J. R. Meteorol. Soc.*, *130*, 1023–1045.

Sterl, A. (2004), On the (in)homogeneity of reanalysis products, *J. Clim.*, *17*, 3866–3873.

Turner, J., S. R. Colwell, G. J. Marshall, T. A. Lachlan-Cope, A. M. Carleton, P. D. Jones, V. Lagun, P. A. Reid, and S. Iagovkina (2005), Antarctic climate change during the last 50 years, *Int. J. Climatol.*, *25*, 279–294.

Turner, J., T. A. Lachlan-Cope, S. Colwell, G. J. Marshall, and W. M. Connolley (2006), Signficant warming of the Antarctic winter troposphere, *Science*, *311*, 1914–1917.

Undén, P., et al. (2002), The High Resolution Limited Area Model, Hirlam-5 scientific documentation, Swed. Meteorol. and Hydrol. Inst., Norrköping, Sweden.

van As, D., and M. R. van den Broeke (2006), Structure and dynamics of the summertime atmospheric boundary layer over the Antarctic Plateau: 2. Heat, moisture and momentum budgets, *J. Geophys. Res.*, *111*, D07103, doi:10.1029/2005JD006956.

van As, D., M. R. van den Broeke, and R. S. W. van de Wal (2005), Daily cycle of the surface layer and energy balance on the High Antarctic Plateau, *Antarct. Sci.*, *17*(1), 121–133, doi:10.1017/S0954102005.

van de Berg, W. J., M. R. van den Broeke, C. H. Reijmer, and E. van Meijgaard (2005), Characteristics of the Antarctic surface mass balance (1958–2002) using a regional atmospheric climate model, *Ann. Glaciol.*, *41*, 97–104.

van de Berg, W. J., M. R. van den Broeke, C. H. Reijmer, and E. van Meijgaard (2006), Reassessment of the Antarctic surface mass balance using calibrated output of a regional atmospheric climate model, *J. Geophys. Res.*, *111*, D11104, doi:10.1029/2005JD006495.

van den Broeke, M. R., and N. P. M. van Lipzig (2003), Factors controlling the near-surface wind field in Antarctica, *Mon. Weather Rev.*, *131*(4), 733–743.

van den Broeke, M. R., and N. P. M. van Lipzig (2004), Changes in Antarctic temperature, wind and precipitation in response to the Antarctic Oscillation, *Ann. Glaciol.*, *39*, 119–126.

van den Broeke, M. R., J.-G. Winther, E. Isaksson, J. F. Pinglot, L. Karlöf, T. Eiken, and L. Conrads (1999), Climate variables along a traverse line in Dronning Maud Land, East Antarctica, *J. Glaciol.*, *45*(150), 295–302.

van den Broeke, M. R., N. P. M. van Lipzig, and E. van Meijgaard (2002), Momentum budget of the East Antarctic atmospheric boundary layer: Results of a regional climate model, *J. Atmos. Sci.*, *59*, 3117–3129.

van den Broeke, M. R., C. H. Reijmer, and R. S. W. van de Wal (2004), Surface radiation balance in Antarctica as measured with automatic weather stations, *J. Geophys. Res.*, *109*, D09103, doi:10.1029/2003JD004394.

van den Broeke, M. R., C. H. Reijmer, D. van As, R. S. W. van de Wal, and J. Oerlemans (2005), Seasonal cycles of Antarctic surface energy balance from automatic weather stations, *Ann. Glaciol.*, *41*, 131–139.

van den Hurk, B., and P. Viterbo (2003), The Torne-Kalix PILPS 2 (e) experiment as a test bed for modifications to the ECMWF land surface scheme, *Global Planet. Change*, *38*, 165–173.

White, P. W. (2001), Part IV, Physical processes (CY23R4), manual, Eur. Cent. For Med.-Range Weather Forecasts, Reading, U. K.

W. J. van de Berg and M. R. van den Broeke, Institute for Marine and Atmospheric Research Utrecht, Universiteit Utrecht, Princetonplein 5, NL-3584 CC, Utrecht, Netherlands. (w.j.vandeberg@phys.uu.nl)

E. van Meijgaard, Royal Dutch Meteorological Institute, NL-3730 AE De Bilt, Netherlands.